Facility Effects on the Ion Characteristics of a 12.5-kW Hall Thruster

Wensheng Huang* and Hani Kamhawi†
National Aeronautics and Space Administration Glenn Research Center, Cleveland, OH, 44135, USA

During a laser-induced fluorescence test of a 12.5-kW magnetically-shielded Hall thruster, ion characteristics in the discharge channel and near the poles were measured as the background pressure and electrical configuration were varied. The acceleration zone of the thruster moved upstream by 2% and 10% of the channel length when the background pressure was raised to 1.8 times and 7 times the lowest achievable pressure, respectively. Examination of the characteristics of the ions near the pole covers suggested that as the background pressure decreased the pole covers may be experiencing more erosion. When operating at a discharge voltage of 300 V, the acceleration zone was observed to be at the same location for all electrical configurations. When operating at a discharge voltage of 600V, the acceleration zone was observed to move 3% of the channel length upstream when the thruster body was floated instead of tied to the cathode or grounded to the facility. Characteristics of the ions bombarding the pole covers did not vary across the tested electrical configurations. This observation combined with thruster body voltage measurements suggested that varying the electrical configuration only affected the thruster body sheath voltage and did not affect the plasma potential beyond the sheath. ‡

Abbreviations

AOI = Angle Of Incidence

FWHM = Full-Width-at-Half-Maximum

HERMeS = Hall Effect Rocket with Magnetic Shielding

* Research engineer, Electric Propulsion Systems Branch, AIAA Associate Fellow, wensheng.huang@nasa.gov.
† Research engineer, Electric Propulsion Systems Branch, AIAA Associate Fellow.
‡ A conference version of this paper was presented at the 2020 AIAA Propulsion and Energy Forum, Aug 24-28, 2020, virtual, AIAA-2020-3616.

IFPC = Inner Front Pole Cover

LIF = Laser-Induced Fluorescence

OFPC = Outer Front Pole Cover

SNR = Signal-to-Noise Ratio

TDU = Technology Development Unit

I. Introduction

During the development of a 12.5-kW Hall thruster, a set of Laser-induced Fluorescence (LIF) tests focused on facility effects were performed. The thruster tested was Hall Effect Rocket with Magnetic Shielding (HERMeS) Technology Development Unit 1 (TDU1). This LIF test studied the characteristics of the ions in the discharge channel as well as near the pole covers. The phenomenon of pole erosion was not previously studied in depth in the Hall thruster community because channel wall erosion was the more immediate life-limiting factor for these devices until the development of magnetic shielding [1-13]. More recently, simulation and experimental work related to pole erosion in magnetically shielded Hall thrusters revealed that the erosion rate may be driven by a combination of cathode ions and discharge channel ions with energy enhanced by lower hybrid plasma waves [14-23].

This article will focus on the tests to study the effects of background pressure and electrical configurations. For an in-depth review of pre-2009 literature related to the effect of background pressure on Hall thrusters, see this review paper [24]. The current article will give a brief review of more recent literature and will cite representative examples where large body of similar works exist.

In past studies, Hall thrusters had been shown to typically exhibit increased performance (e.g. efficiency, specific impulse) with increasing background pressure [24-36], though there are also instances where performance was observed to decrease at very high background pressure (40-50 micro-Torr) [25, 37]. This phenomenon is attributed to the ingestion of background neutral particles. Note that in the framework of background neutral ingestion, thrust is typically observed to increase with background pressure when the thruster anode flow rate is fixed because the additional ingested flow is ionized and generates additional thrust [25, 26, 30]. However, when the flow rate is varied to maintain constant discharge power, thrust has been observed to increase [29, 31, 32, 34], hold constant [30, 32], or decrease [32, 37, 38] with background pressure depending on the thruster, operating condition, and test setup. This may be attributed to a competition between the increased thrust from neutral ingestion and the decreased thrust

from decreasing the thruster flow rate to maintain constant discharge current. Another possibility is that the change in background neutral flow field directly impacts the electron mobility profile, which can lead to increase or decrease in thrust [30, 35, 36]. Experimental and modeling work showed that the effect of ingestion is not a linear process. Ingestion rate is driven by the flux (not just density) of background neutrals resulting from the geometries of the vacuum facility and pumping surfaces [33, 39]. At very low background pressure, the collision frequencies in the plume are low enough that the ingestion rate and associated effect on performance metrics are roughly linear with the background pressure. However, at elevated background pressure, some background neutrals are scattered in interactions with the plume and the facility, leading to non-linear behavior [33, 39]. These non-linear interactions can lead to leveling off in different performance metrics with rising background pressure [29, 33]. Complex interactions in the plume and with the facility can also give rise to non-Maxwellian distributions on the ingested gas [39] such that simple models of ingestion tend to be inaccurate [28]. Furthermore, trends in thruster-cathode coupling with background pressure depend on whether the cathode is centrally or externally located [30, 40, 41]. For thrusters with externally mounted cathodes, whether the cathode is located inside or outside the separatrix [42, 43] and collisions with background neutrals appear to influence the coupling of the cathode electrons to the main discharge plasma. For a facility with conducting walls, cathode electrons may find alternate pathways to recombine with the ions in processes that may be linked to the presence of background neutrals [44-46]. Thrusters with externally-mounted cathodes have also displayed more sensitivity to background pressure variations, particularly with regards to discharge oscillation characteristics [37]. The use of centrally-mounted cathodes is shown to mitigate jumps in thruster behavior due to changing thruster-cathode coupling but does not prevent the effects of background neutral ingestion [30, 38].

In past background pressure studies involving LIF, the acceleration zone of the Hall thruster operating on xenon had been found to move upstream with increasing background pressure [47-51]. There was also an example where a Hall thruster operating on krypton did not display measurable change with increasing background pressure [52]. Notably, the amount by which the acceleration zone recedes upstream as background pressure rises has been observed to level off at high background pressure [50, 51]. Since the acceleration profile of a Hall thruster is directly linked to its electron mobility profile, the aforementioned observations may also be interpreted as evidence that ingestion of background neutrals affect the electron mobility profile of a Hall thruster. LIF test data presented in the current article will show how the acceleration zone of the HERMeS varied with background pressure.

In past studies of the HERMeS, the thruster body current and voltage were found to be similar in magnitude when the body was grounded to the facility versus tied to the cathode but very different when the body was electrically floated [53]. Based on the fact that no facility would be present to ground the thruster body to in flight, HERMeS was designed to nominally operate with the cathode electrically tied to the body. The configuration of cathode-tied-to-body was chosen over floating body because the body voltage became several tens of eV more negative and body voltage oscillation peak-to-peak grew by a factor of 4 when the body was floated [53]. An assumption was made that the effect of the electrical configuration does not reach beyond the sheath of the thruster body and does not alter the overall ion flow field leading up to the sheath. Given this assumption, differences in energy of the ions bombarding the pole cover should be approximately equal to the difference in the body voltage between the floating body and the cathode-tied-to-body configurations. LIF test data presented in the current article will assess the validity of this assumption.

II. Experimental Setup

The experimental setup is the same as described in a prior article [18] and a brief overview is given below for convenience.

A. Thruster and Test Matrix

Testing was performed on the HERMeS TDU1, which was designed to be a 12.5 kW, 3000 s, magnetically-shielded Hall thruster [54]. Tested thruster operating conditions are listed in Table 1. The cathode mass flow rate was maintained at 7% of the anode mass flow rate. All results reported in this article are operations at nominal magnetic field strength, which corresponds to magnetic shielding topology with margin against oscillation mode transitions. Fig. 1 shows a photo of the HERMeS TDU1 on the LIF test stand.

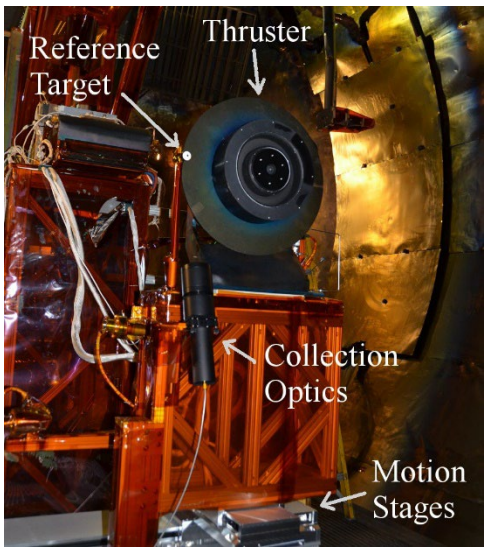

Fig. 1. HERMeS TDU1 on test stand.

For the testing described in this article, the thruster body was isolated from the test stand and electrically connected to the cathode except during the electrical configuration study. During the electrical configuration study, the three tested configurations were thruster body

tied to cathode common, floating thruster body, and thruster body grounded to facility ground.

To simplify plot labeling, throttle points are labeled by discharge voltage and discharge power. A label that says "600-12.5" refers to the throttle point with a discharge voltage of 600 V and a discharge power of 12.5 kW. For the background pressure study, labels for the operating condition additionally include "Pp.p", which refers to the ratio of the background pressure to the minimum pressure achieved. For example, "600-12.5-P1.8" refers to the 600 V, 12.5 kW operating condition with a background pressure that is 1.8 times that of the minimum background pressure. Operating conditions for the electrical configuration study are labeled with a suffix corresponding to the configuration tested. For example, "600-12.5-CB" refers to the 600 V, 12.5 kW operating condition where the cathode is tied to the thruster body, "600-12.5-Flt" refers to the body being floated, and "600-12.5-Gnd" refers to the body being grounded to the facility ground.

For this article, all spatial positions around the thruster are normalized based on the region of interest. For the thruster discharge channel, radial positions are normalized by the discharge channel width, where R = 0 is the inner wall and R = 1 is the outer wall. Similarly, data near the inner and outer front pole covers are normalized so that R = 0 and R = 1 correspond to the inner and outer radial edges, respectively, of the region of interest. Fig. 2 is a cross sectional diagram showing the relative positions of the regions of interest. The radial position corresponding to R = 0 and R = 1 are marked for each region. For all regions, axial positions are normalized by the discharge channel length, which is defined as the axial distance from the anode downstream surface to the exit plane as defined by the inner front pole cover downstream surface. Z is set to 0 at the exit plane and is positive in the downstream direction.

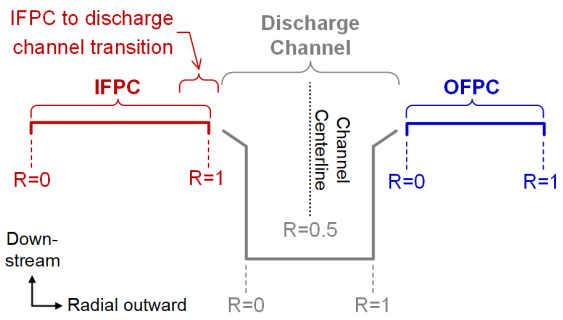

Fig. 2. Cross sectional diagram depicting the relative locations of the regions of interest.

B. Test Facility

The LIF test stand can move the thruster horizontally in the radial and axial directions. Propellant and electrical feeds were designed to accommodate the motion of the test stand.

Two ion gauges, calibrated on xenon, monitor the background pressure near the thruster. Gauge readings were corrected for temperature and pointing relative to background flux via methods described in Yim and Burt [39]. Total uncertainty in pressure is estimated to be 10% to 15% of the reading. Table 1 lists the label, discharge voltage, discharge power, and background pressure near the thruster for the tested operating conditions. The listed background pressure near the thruster is the average over the two ion gauges and over the duration of each operating condition.

Table 1. Background pressure near thruster for tested operating conditions.

Label	Discharge voltage, V	Discharge power, kW	Background pressure near thruster, micro-Torr
300-2.4-P1.0	300	2.40	5.2
300-2.4-P2.0	300	2.40	10
300-2.4-P3.4	300	2.40	18
300-2.4-P5.0	300	2.40	26
300-2.4-P7.0	300	2.40	36
300-6.3-P1.0	300	6.25	12
300-6.3-P1.3	300	6.25	16
300-6.3-P1.8	300	6.25	22
600-12.5-P1.0	600	12.50	12
600-12.5-P1.3	600	12.50	16
600-12.5-P1.8	600	12.50	21

Background pressure was elevated by injecting supplementary xenon gas downstream of the thruster with typical uncertainty of ±1% of target. Due to equipment limitations, up to 7x the lowest background pressure was achieved for the 300 V, 2.4 kW condition and up to 1.8x the lowest background pressure for the other tested conditions. Propellant flow to the thruster was adjusted as needed to maintain constant discharge current and fixed cathode flow fraction as the background pressure was varied. Electrical connections leading to the thruster body, cathode common, and facility ground were isolated from each other and accessible on the air side of the facility. Changing the electrical configuration was accomplished by re-configuring these electrical connections with appropriate jumper cables.

C. Diagnostics

The LIF velocimetry scheme used in this test excited the XEII 834.953 nm (vac) transition and collected fluorescence from the 542.066 nm (vac) transition [55]. In prior work, the hyperfine structure of this transition was studied and the highest quality data can be produced by using pi-polarization on the axial laser injection axis and sigma-polarization on the side injection axes [18, 56]. Corrections for Zeeman Effect on the side axes data are performed in post-processing using a linear model developed in a prior work [56].

Fig. 4 shows a diagram of the optics setup inside the vacuum facility. Part (a) of the figure shows the three sets of injection optics that were deployed. Optical fibers were used to deliver laser light to each set of injection optics. A saturation study was performed, and laser power delivered to each axis was set to keep the maximum broadening in the velocity distribution functions to below 10%. The thruster was mounted to motion stages that provided radial

and axial movements. A reference target was mounted at a known distance from the thruster in the same plane as the three injected laser beams. Part (b) of the figure shows the collection optics that were mounted 70° out of the injection plane. An optical fiber was used to deliver fluorescence light out of the vacuum facility, where a set of electronics filter out the meaningful portion of the signal from the background noise. The characteristic spatial resolution was approximately 1 mm in size, set by the beam waist of the injection beams and the viewing cone of the collection optics.

More details regarding treatment of the Zeeman Effect, laser alignment, and signal processing can be found in a prior publication [18].

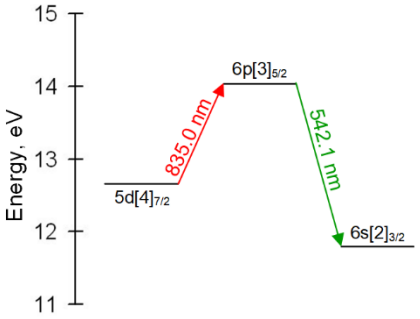

Fig. 3. Transition diagram for Xe II LIF at 834.953 nm (vac).

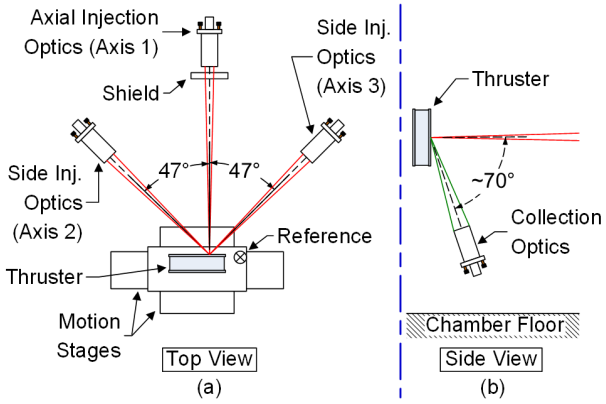

Fig. 4. Top view (a) and side view (b) of vacuum-side optical setup.

III. Data Analysis

A. LIF Data Analysis Method

The analysis of the LIF data was divided into four steps. In step one, the wavelength reference data were converted into a velocity scale. In step two, the intensity data were corrected for laser power variations. In step three, skew-normal, Gaussian, and two-Gaussian curve-fits were performed while accounting for Zeeman Effect on the hyperfine structure for the XEII 834.953 nm (vac) transition.[56] An examination of the initial skew-normal curve-fits was used to identify the rough boundaries of the acceleration region, which was defined as the region where the magnitude of averaged ion velocity was between 10% and 90% of the maximum magnitude of the ion velocity. In regions downstream of the upstream boundary of the acceleration zone, the coefficient of determination (also known as the R squared value) and the concavity of the curve-fits were used to determine whether there were more than one ion populations present. For velocity distributions that show only one peak, skew-normal curve-fit generally give

better R squared values than Gaussian curve-fit when the signal-to-noise ratio (SNR) was greater than 4. When the SNR was less than 4, skew-normal fit can fit long tails that have lower magnitude than the magnitude of the noise. To avoid the fitting of tails that may not be real, Gaussian fit was reported instead of skew-normal fit when SNR was less than 4. When more than one ion populations were present, data from the three laser axes allowed a unique determination of which of the two peaks on each axis is associated with each other. A detailed description of the methodology for velocity distribution curve-fits and the use of three laser axes to extract distribution data in the presence of more than one ion population can be found in a prior publication [18].

For the final step of the LIF data analysis, energy distribution function of each identified ion population was constructed using the Monte Carlo method. The energy distribution functions were then used to calculate the averaged energy and full-width-at-half-maximum (FWHM) energy. The percentage of the population with energy in excess of a threshold energy of 50 eV was also calculated. More detail about the associated methodology and calculations can be found in a prior publication [18].

B. Uncertainty Analysis

The uncertainty in position was dominated by the size of the interrogation zone and the drift in alignment of the optics. The alignment procedure used in this LIF test rejected data where alignment drifted by more than 0.5 mm from the reference.

The signal-to-noise ratio, defined as the ratio of the peak signal divided by the standard deviation of the noise, was used to assess the uncertainty in the data. Using an assessment of the data set, an SNR value of 3 was set as the level below which data was considered statistically insignificant. This assessment showed that the uncertainties were typically within ±100 m/s but could be as high as ±600 m/s for scans with low SNR (SNR slightly higher than 3). The wavemeter and optogalvanic cell combination additionally contribute an uncertainty of ±50 m/s. The effective total uncertainty was ±112 m/s for most scans and up to ±600 m/s for scans with low SNR.

To decrease uncertainty at a cost of spatial resolution, averages over multiple data locations are performed in the results section. Assuming four samples are available for each averaged quantity and conservatively a maximum uncertainty of 600 m/s for each sample, standard error propagation is used to provide conservative estimates of the uncertainties in the averaged quantities. For the reported averaged energy, the uncertainty ranged from ±4 eV when at 30 eV (typical energy found near the inner pole) and ±6 eV when at 130 eV (typical energy found near the outer pole). For the reported averaged angle of incidence, the uncertainty was up to ±6° for all regions. Note that all

measured ion distribution functions exhibited spread, as characterized by the FWHM energy, that is typically five to ten times as large as the measurement uncertainty. Specific values of uncertainties for data presented in this article are available upon reasonable request.

IV. Results

A. Background Pressure Study

To facilitate discussions, the region near the inner front pole cover will be referred to as the IFPC and the region near the outer front pole cover will be referred to as the OFPC.

Fig. 5 shows the averaged axial ion velocity along the channel centerline for the background pressure study at the 300 V, 6.3 kW operating condition. Fig. 6 shows the same for the 300 V, 2.4 kW condition. Although the tested pressure range for the 300 V, 6.3 kW and 600 V, 12.5 kW conditions were small, a check against the velocity uncertainty and the spatial resolution shows that the detected upstream movements of the acceleration zone were statistically significant. Defining the acceleration zone location as the point along the discharge channel centerline where the averaged axial ion velocity reached half of the maximum magnitude of ion velocity, the acceleration zone location moved upstream by 2% of the channel length when the background pressure was raised to 1.8 times the lowest achievable for the operating conditions of 300 V, 6.3 kW and 600 V, 12.5 kW. For data from 300 V, 2.4 kW operations, the acceleration zone location moved upstream by 10% of the channel length when the background pressure was raised to 7 times the lowest achievable. Variations in acceleration zone location were comparable for background pressures up to ~20 micro-Torr for all three operating conditions (roughly equal to 1.8X for 300-6.3 and 600-12.5 operations and 3.4X for 300-2.4 operations). This result is in good agreement with prior background pressure effect studies looking at the performance parameters of the HERMeS TDU, where changes in thrust were observed to be <3% for pressure up to 20 micro-Torr at these discharge voltages [38].

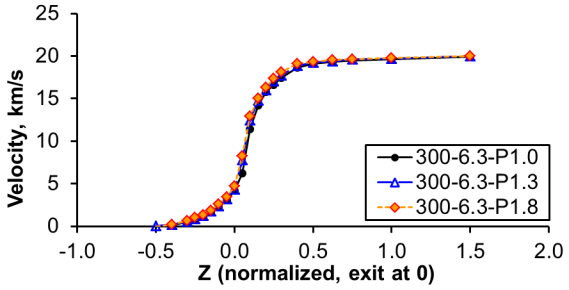

Fig. 5. Averaged axial velocity along the channel centerline for operations at 300 V, 6.3 kW.

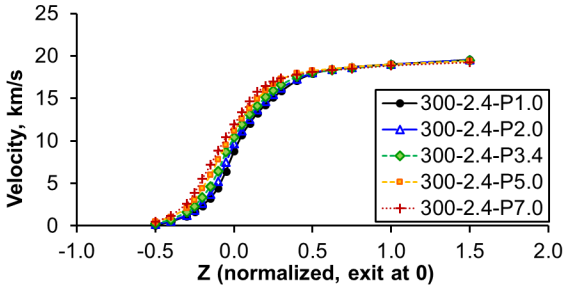

Fig. 6. Averaged axial velocity along the channel centerline for operations at 300 V, 2.4 kW.

Fig. 7 and Fig. 8 show the averaged velocity vectors near the IFPC and OFPC, respectively, for the thruster operating at 300 V, 6.3 kW and different background pressures. Fig. 9 and Fig. 10 show the same near the IFPC and OFPC, respectively, for the thruster operating at 300 V, 2.4 kW. The 600 V, 12.5 kW condition exhibited trends similar to the 300 V, 6.3 kW condition. For the IFPC ion vector plots, the red arrows represent ions originating from the discharge channel, the blue arrows represent ions originating from the cathode, and any black arrows indicate that only one population was identified at those locations. The origin of each population was identified by tracing the ion vectors backward. Detailed methodology can be found in a prior publication [18]. Due to overlapping nature of the velocity distribution functions of different ion populations, some of the black arrows shown in the IFPC plots may represent averages over more than one ion populations. Note that IFPC data were not collected for the 300-2.4-P3.4 operating condition due to limited test time. For 300 V, 6.3 kW and 600 V, 12.5 kW, the ion velocity vectors were constant to within measurement uncertainty over the range of tested pressures. For 300 V, 2.4 kW, where the tested background pressure range was relatively large, there was a statistically significant decrease in the magnitude of averaged ion velocity as the background pressure increased.

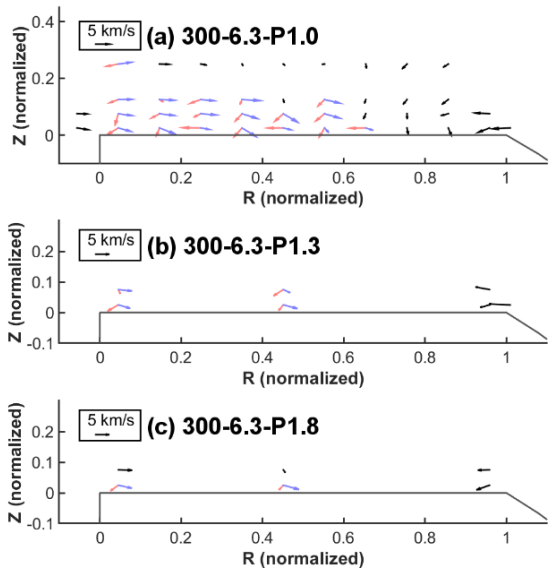

Fig. 7. Averaged velocity vector near the IFPC for 300 V, 6.3 kW operations with (a) 1x, (b) 1.3x, (c) 1.8x minimum background pressure.

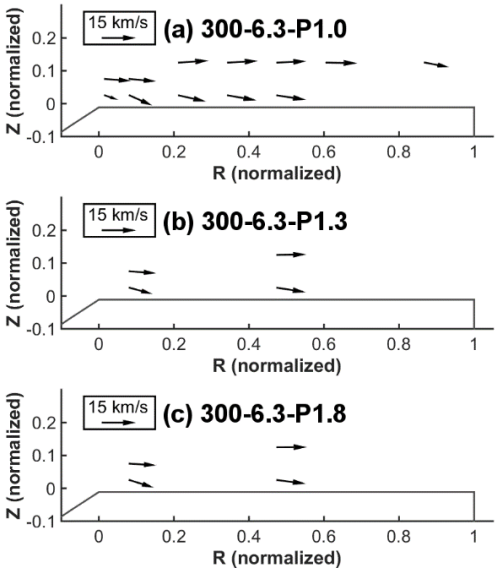

Fig. 8. Averaged velocity vector near the OFPC for 300 V, 6.3 kW operations with (a) 1x, (b) 1.3x, (c) 1.8x minimum background pressure.

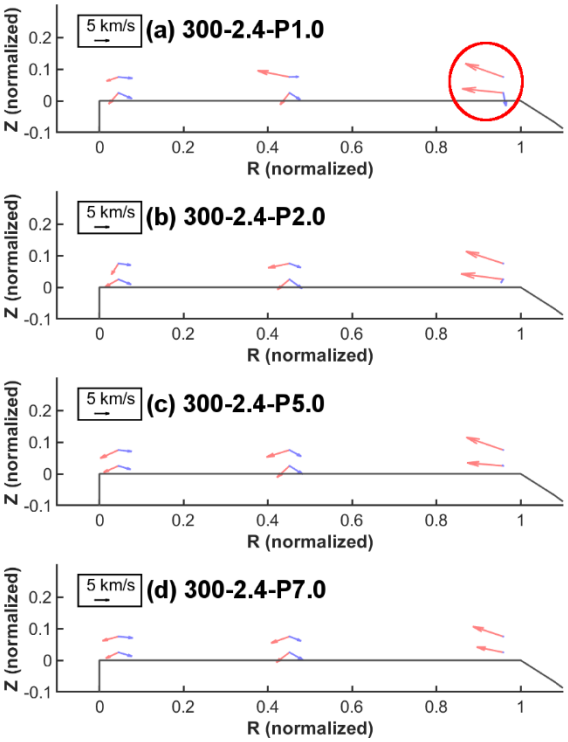

Fig. 9. Averaged velocity vector near the IFPC for 300 V, 2.4 kW operations with (a) 1x, (b) 2x, (c) 5x, and (d) 7x minimum background pressure.

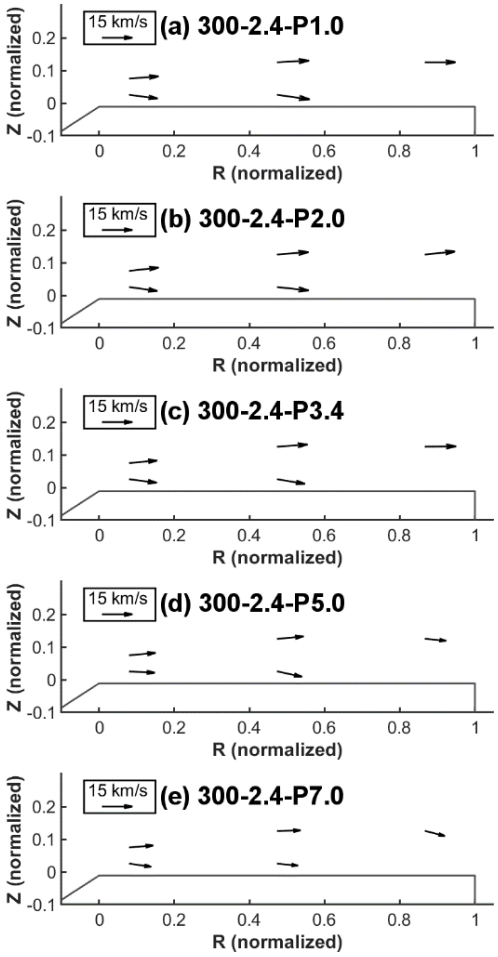

Fig. 10. Averaged velocity vector near the OFPC for 300 V, 2.4 kW operations with (a) 1x, (b) 2x, (c) 3.4x, (d) 5x, and (e) 7x minimum background pressure.

To quantify the behavior of the ions near the pole covers, the energy and direction parameters were calculated. Table 2 summarizes the averaged ion energy, FWHM energy, percentage of population with more than 50 eV, and averaged angle of incidence (abbreviated as AOI in the table) with respect to the IFPC surface normal for the background pressure study. Given the low SNR for pole cover data in general, the results in this table were averaged across locations near the IFPC where the two counter-streaming ion populations could be separated for each operating condition. This approach provided better statistical confidence at a cost of spatial details. For reasons that will be explained later, the transition region from the IFPC to the discharge channel chamfer (region in red circle in Fig. 9a) was left out of the averaging done for Table 2 and put in a separate table. Table 3 summarizes the ion characteristics near the OFPC. Table 4 summarizes the energy characteristics at the location that represents the

transition from the IFPC to the discharge channel (red circle in Fig. 9a). For Table 3, no values were tabulated for 600 V, 12.5 kW operations due to low SNR. For Table 4, no values were tabulated for 300 V, 6.3 kW and 600 V, 12.5 kW operations due to low SNR.

Table 2. IFPC ion characteristics for the background pressure study.

		Discharge Channel Stream				Cathode Stream			
Operating Condition	Sample Size	E_{AVG}, eV	E_{FWHM}, eV	% above 50 eV	AOI_{AVG}, degree	E_{AVG}, eV	E_{FWHM}, eV	% above 50 eV	AOI_{AVG}, degree
300-6.3-P1.0	13	24	21	6.5	48	30	32	15.5	66
300-6.3-P1.3	4	24	19	9.8	45	26	26	8.8	70
300-6.3-P1.8	2	17	13	3.4	41	29	29	8.4	72
600-12.5-P1.0	11	22	23	3.7	43	27	29	10.2	61
600-12.5-P1.3	4	22	25	4.1	61	19	20	5.1	79
600-12.5-P1.8	4	24	26	4.9	48	29	33	11.4	66
300-2.4-P1.0	4	56	47	42.9	59	27	30	11.1	71
300-2.4-P2.0	4	43	49	27.2	49	29	34	15.6	63
300-2.4-P5.0	4	55	71	42.8	57	33	38	18.1	64
300-2.4-P7.0	4	40	45	29.0	60	31	40	18.1	67

Table 3. OFPC ion characteristics for the background pressure study.

Operating Condition	Sample Size	E_{AVG}, eV	E_{FWHM}, eV	% above 50 eV	AOI_{AVG}, degree
300-6.3-P1.0	8	119	77	98.4	84
300-6.3-P1.3	3	102	88	91.0	83
300-6.3-P1.8	4	112	78	97.7	82
300-2.4-P1.0	5	175	91	100	88
300-2.4-P2.0	5	171	98	99.9	90
300-2.4-P3.4	5	161	118	99.3	88
300-2.4-P5.0	5	132	119	96.2	88
300-2.4-P7.0	5	104	106	87.6	85

Table 4. Discharge channel stream characteristics near the transition from the IFPC to the discharge channel for the background pressure study.

Operating Condition	E_{AVG}, eV	E_{FWHM}, eV
300-2.4-P1.0	160	97
300-2.4-P2.0	163	115
300-2.4-P5.0	140	100
300-2.4-P7.0	97	113

From Table 2 and Table 3, one can see that operations at low discharge current (300 V, 2.4 kW) corresponded to ions arriving at the poles with higher energies than operations at high discharge current (300 V, 6.3 kW and 600 V, 12.5 kW). Furthermore, in the IFPC to discharge channel transition region (IFPC R = 0.96), energetic ions were readily detected for low discharge current operation but not for high discharge current operations.

Comparing Table 3 and Table 4, one can see that the ion energy characteristics near the OFPC and the IFPC to discharge channel transition regions are very similar. Ion vectors in these regions (Fig. 9 and Fig. 10) have similar length and are pointing away from the discharge channel suggesting that they may be the same type of energetic ions. Subsequent testing on an engineering successor to the HERMeS TDU confirmed the existence of similar energetic ion populations at a range of 300 V operating conditions [20].

The characteristics of the ions bombarding most of the IFPC, shown in Table 2, do not change appreciably with background pressure with the notable exception of the IFPC to discharge channel transition region as shown in Table 4 (IFPC R = 0.96). For the OFPC region, at the 300 V, 6.3 kW condition, ions exhibited minimal variation over the tested pressure range of 1.8X. In contrast, at the 300 V, 2.4 kW condition, ions exhibited noticeable variations over a range in background pressure of 7X. Energy characteristics at the IFPC to discharge channel transition region were in excellent agreement with the energy characteristics near the OFPC. The averaged energy decreased by approximately 40% at these locations when comparing measurements made at 7X background pressure to 1X background pressure. Notably, this trend was occurring while the acceleration zone was moving upstream with increasing background pressure as shown in Fig. 6.

B. Electrical Configuration Study

Fig. 11 shows the averaged axial ion velocity along the channel centerline for the electrical configuration study at the 300 V, 6.3 kW operating condition. Fig. 12 shows the same for the 600 V, 12.5 kW operating condition. For the 300 V, 6.3 kW operating condition, the acceleration zone location was constant to within measurement uncertainty for all tested electrical configurations. For the 600 V, 12.5 kW operating condition, the acceleration zone location moved upstream by 3% of the channel length when the thruster body was floated compared to when the thruster body was either tied to the cathode or grounded to the facility.

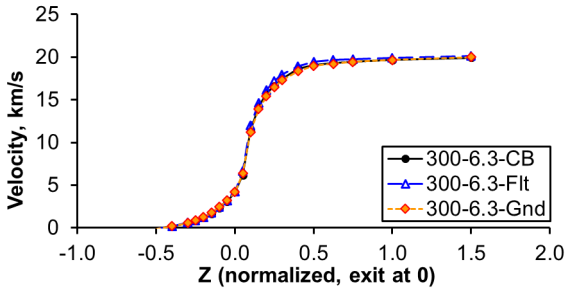

Fig. 11. Averaged axial velocity along the channel centerline for operations at 300 V, 6.3 kW and with different electrical configurations.

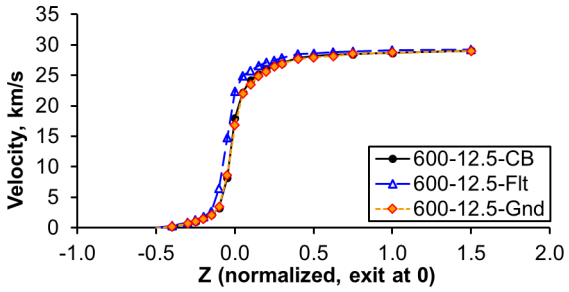

Fig. 12. Averaged axial velocity along the channel centerline for operations at 600 V, 12.5 kW and with different electrical configurations.

Fig. 13 and Fig. 14 show the averaged velocity vectors near the IFPC and OFPC, respectively, for the thruster operating at 300 V, 6.3 kW and different electrical configurations. Fig. 15 show the same near the IFPC for the thruster operating at 600 V, 12.5 kW. For 600 V, 12.5 kW operations, SNR of the OFPC data were too low.

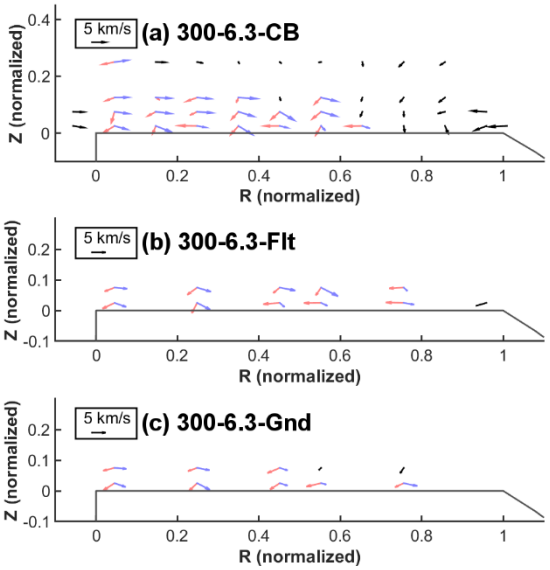

Fig. 13. Averaged velocity vector near the IFPC for 300 V, 6.3 kW operations with different electrical configurations.

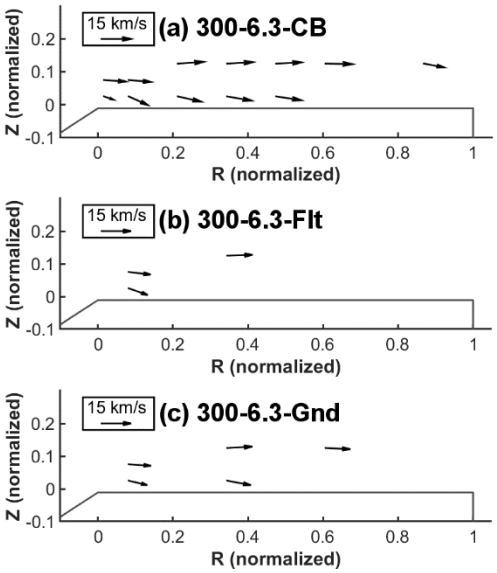

Fig. 14. Averaged velocity vector near the OFPC for 300 V, 6.3 kW operations with different electrical configurations.

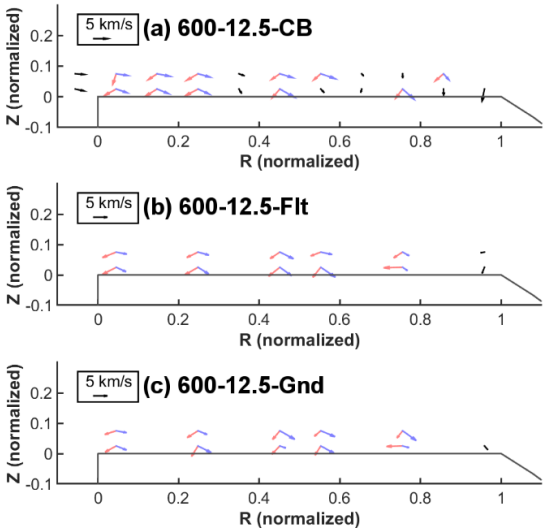

Fig. 15. Averaged velocity vector near the IFPC for 600 V, 12.5 kW operations with different electrical configurations.

Table 5. Thruster body voltage and current during the electrical configuration study.

Operating Condition	Body Voltage, V	Body Current, A
300-6.3-CB	-12.7	0.61
300-6.3-Flt	-32.1	0.00
300-6.3-Gnd	0.0	1.88
600-12.5-CB	-11.6	1.60
600-12.5-Flt	-40.2	0.00
600-12.5-Gnd	0.0	3.00

Table 6. IFPC ion characteristics for the electrical configuration study.

Operating Condition	Sample Size	Discharge Channel Stream E_{AVG}, eV	E_{FWHM}, eV	% above 50 eV	AOI_{AVG}, degree	Cathode Stream E_{AVG}, eV	E_{FWHM}, eV	% above 50 eV	AOI_{AVG}, degree
300-6.3-CB	13	24	21	6.5	48	30	32	15.5	66
300-6.3-Flt	10	25	26	6.0	61	28	28	13.8	62
300-6.3-Gnd	8	22	27	5.3	59	22	26	7.2	70
600-12.5-CB	11	22	23	3.7	43	27	29	10.2	61
600-12.5-Flt	10	26	28	7.3	55	29	31	15.6	58
600-12.5-Gnd	10	23	23	4.9	45	28	28	12.8	61

Table 7. OFPC ion characteristics for the electrical configuration study.

Operating Condition	Sample Size	E_{AVG}, eV	E_{FWHM}, eV	% above 50 eV	AOI_{AVG}, degree
300-6.3-CB	8	119	77	98.4	84
300-6.3-Flt	3	107	90	92.5	81
300-6.3-Gnd	5	110	81	94.5	84

Table 8. Plasma potential measured around the thruster in a related plasma plume study [38].

Operating Condition	Plasma potential at different angles from firing axis, V At -90°	At -45°	At 0°	At 45°	At 90°
300-6.3-CB	4.0	5.8	12.0	5.4	4.5
300-6.3-Flt	3.9	5.8	11.3	5.8	3.9
300-6.3-Gnd	4.0	5.9	12.3	5.5	4.0
600-12.5-CB	4.0	5.9	13.5	5.4	4.0
600-12.5-Flt	4.0	5.8	12.8	5.4	4.5
600-12.5-Gnd	4.1	5.4	12.9	5.4	4.0

Table 5 summarizes the thruster body voltage and current measured during the electrical configuration study. The graphite pole covers were electrically tied to the thruster body. Table 6 summarizes the averaged ion energy, FWHM energy, percentage of population with more than 50 eV, and averaged angle of incidence with respect to the IFPC surface normal for the background pressure study. Table 7 does the same for the OFPC. In a related plasma plume study [38], plasma potential measurements were taken at 1.5 m away from the thruster at a variety of angles from the firing axis. A portion of the plasma potential measurements are shown in Table 8.

From Fig. 13 to Fig. 15 and Tables 6 to 7, one can see that the ion characteristics near the pole covers were largely identical across electrical configurations. Furthermore, Table 8 show that the plasma potentials around the thruster did not change across electrical configurations. Table 5 shows that for the floating body configuration the sheath voltage was on the order of -30 to -40 V with respect to the facility ground. Since the total voltage drop across the sheath of the pole covers was from the local plasma potential to the sheath potential, the total voltage drop would have been in the range of 40 to 60 V in magnitude. The fact that there was no large energy difference between

the near-pole ions measured for the floating body configuration when compared to other configurations implied that the LIF measurements occurred outside of the sheath. In other words, the ions measured by LIF had not undergone any acceleration associated with the sheath voltage drop. As a rough check, using densities and temperatures from a simulation of the TDU operating at 300 V, 6.3 kW [19], the Debye length at the radial middle of the IFPC normalized to the same axial scale as all other axial coordinates is ~0.001. In contrast, the axially closest LIF data location to the IFPC is ~0.03 away on the same normalization scale. This supports the observation that the LIF measurements occurred outside of the bulk of the sheath voltage drop. Given the LIF measurements occurred outside of the sheath voltage drop, one can also conclude that the three electrical configurations tested had minimal impact on the characteristics of the ions arriving at the plasma sheathe over the pole covers.

V. Discussions

Data from this LIF study showed that this 12.5-kW magnetically shielded Hall thruster exhibited many of the same trends as unshielded Hall thrusters when exposed to varying background pressure. In particular, past LIF studies on unshielded [47-49, 51] and shielded [50] Xenon Hall thrusters of power levels ranging from 0.6 kW to 9 kW have observed the acceleration zone moving upstream with increasing background pressure. Data from this study reinforce the notion that magnetically shielded Hall thrusters have the same susceptibility to ingestion as unshielded thrusters and the location of the acceleration zone exhibit the same trends with background pressure.

As seen in the results, the averaged energy of the ions bombarding the IFPC were different from that bombarding the OFPC (20-55 eV and 100-175 eV, respectively) with the notable exception that in the IFPC to discharge channel transition region the ion energies match closely to those bombarding the OFPC. A possible explanation for this behavior is that the ions bombarding the OFPC and IFPC to discharge channel transition regions were energized by one mechanism while the ions bombarding the remainder of the IFPC were driven by a different mechanism. For example, works by Mikellides and Lopez Ortega pointed to the possibility of lower hybrid plasma waves at work near the poles of magnetically shielded Hall thrusters [17, 19] that enhanced the energy of the ions. Two types of plasma waves were studied by Mikellides and Lopez Ortega, the modified two-stream instability and the lower hybrid drift instability, and they have different growth equations as well as conditions under which each can dominate. In this theoretical framework, observations of starkly different ion characteristics over different regions of the inner pole may be evidence that different plasma waves dominated each region. There is the possibility that ions

from the centrally mounted cathode dramatically altered the conditions over most of the inner pole, leading to one type of wave mechanism being dominate, but that near the discharge channel the relatively low density of cathode ions led to conditions being driven by only the discharge channel ions and therefore another type of wave mechanism was dominate. Though not an exhaustive list, other candidates for plasma waves that can be driving the characteristics of the ions over the IFPC include electron cyclotron drift instability, ion acoustic instability, and ion-ion two-stream instability [57-59]. Any one or a combination of the aforementioned instabilities can lead to ion characteristics being different over the IFPC when compared to the OFPC and IFPC to discharge channel transition region.

Another observation from the background pressure study was that the energy of the ions bombarding the poles decreased with increasing background pressure and this occurred while the acceleration zone moved upstream. One hypothesis is that the ions were grazing the discharge channel chamfers at 300-2.4-P1.0, such that further movement of the acceleration zone upstream as the background pressure increased caused more of the high-energy ions to impact the discharge channel chamfers and less of them to arrive at the poles. Another possibility is that the high energy in the ions observed in the transition region between the IFPC and the discharge channel and near the OFPC were due to plasma wave heating, as previously described, and the rise in background neutral density had a moderating effect on the plasma wave heating. Subsequent data taken from the engineering successor to the HERMeS [20] imply that the latter hypothesis is more likely to be true. The engineering unit was previously shown to behave identically to the HERMeS [20, 60]. During engineering unit LIF test, a higher SNR (factor of 2-3) was achieved in measurements near the pole. Three ion populations were identified in the IFPC to discharge channel transition region when the thruster operated at the 300 V, 3 kW and 300 V, 6.3 kW conditions. Of these populations, one was identified as cathode ions while the other two were from the discharge channel. Of the discharge channel populations, one was found to be more focused (beam-like) and more like the ions in middle of the discharge channel while the other was more like the ions measured near the OFPC. By studying the beam-like discharge channel population, one can conclude that the acceleration zone was not near the discharge channel chamfer [20]. If the data from the engineering unit LIF test was correctly interpreted, the latter hypothesis is favored over the former hypothesis and the wear of the pole covers will increase with decreasing background pressure. A wear study at different background pressure was carried out on the HERMeS while operating at 5 and 12 micro-Torr background pressure [22]. The results of this study show that the pole cover wear rates were different at different pressures but

not in a statistically significant manner. Longer duration tests with larger difference in background pressure may provide more definitely assessments of how pole cover erosion varies with background pressure. Measurements of ion densities near the poles to complement the LIF energy measurements would also provide great insights into this phenomenon.

Assuming that the energies of the ions near the OFPC and IFPC to discharge channel transition regions are driven by one instability and that of the ions near the rest of the IFPC are driven by a different instability, an accurate model of Hall thruster pole cover erosion will need to be able to predict when each mechanism dominates. If interactions between multiple ion populations affect the type of instabilities present and the energies of the ions bombarding the pole, then the ability to simulate multiple ion populations is likely necessary for accurate predictions. For the particular case of IFPC erosion in a Hall thruster with centrally mounted cathode, an erosion model may need to be able to simulate the coupling between the discharge channel ion population with the cathode ion population as opposed to treating them as independent populations.

VI. Conclusions

During the HERMeS TDU1 LIF test, trends in ion acceleration characteristics were measured as the background pressure and electrical configuration were varied.

Examination of the data from the background pressure study showed that the acceleration zone of the 12.5-kW Hall thruster moved upstream with increasing background pressure. At 1.8 times the lowest achievable pressure, the amount of movement was 2% of the channel length and energy of the ions bombarding the pole covers was roughly constant to within measurement uncertainty. At 7 times the lowest achievable pressure and when operating at low power (300 V, 2.4 kW), the acceleration zone moved upstream by 10% of the channel length. At the same operating condition, the averaged energy of the ions bombarding the inner front pole cover decreased by ~30% while the averaged energy of the ions bombarding the inner pole to discharge channel transition region and the outer front pole decreased by ~40% when compared to at the lowest achievable pressure. In theory, the upstream movement of the acceleration zone with increasing background pressure should bring more energetic ions closer to the poles. At the same time, high energy ions produced by plasma wave heating should experience a decrease in energy as the increased number of background neutrals moderate the plasma waves. Available data favors the latter hypothesis,

which implies that the erosion of the poles will increase with decreasing background pressure. However, more studies are needed to provide certainty.

Examination of the data from the electrical configuration study showed that the acceleration zone location was largely constant between the configuration of cathode-tied-to-body and grounded body. The acceleration zone appeared to shift slightly upstream when the body was electrically floated. The characteristics of the ions bombarding the poles were found to be constant to within measurement uncertainty across the electrical configurations, implying that the LIF data were not affected by changes in the thruster body voltage with changing electrical configuration. These data support the hypothesis that varying the electrical configuration of the thruster body did not affect the plasma potential and ion characteristics outside of the thruster body plasma sheath.

Acknowledgments

This work was supported by NASA's Space Technology Mission Directorate through the Solar Electric Propulsion project. Testing was performed in Vacuum Facility 6 at the NASA Glenn Research Center.

References

[1] Mikellides, I. G., Katz, I., Hofer, R. R., Goebel, D. M., de Grys, K., and Mathers, A. J., "Magnetic Shielding of the Channel Walls in a Hall Plasma Accelerator", *Physics of Plasmas*, Vol. 18, No. 3, Mar 8, 2011, pp. 033501.
https://doi.org/10.1063/1.3551583

[2] Mikellides, I. G. and Katz, I., "Numerical Simulations of Hall-Effect Plasma Accelerators on a Magnetic-Field-Aligned Mesh", *Physical Review E*, Vol. 86, No. 4, Oct 17, 2012, pp. 046703.
https://doi.org/10.1103/PhysRevE.86.046703

[3] Mikellides, I. G., Katz, I., Hofer, R. R., and Goebel, D. M., "Magnetic Shielding of Walls from the Unmagnetized Ion Beam in a Hall Thruster", *Applied Physics Letters*, Vol. 102, No. 2, Jan 17, 2013, pp. 023509.
https://doi.org/10.1063/1.4776192

[4] Mikellides, I. G., Katz, I., Hofer, R. R., and Goebel, D. M., "Magnetic Shielding of a Laboratory Hall Thruster. I. Theory and Validation", *Journal of Applied Physics*, Vol. 115, No. 4, Jan 24, 2014, pp. 043303.
https://doi.org/10.1063/1.4862313

[5] Hofer, R. R., Goebel, D. M., Mikellides, I. G., and Katz, I., "Magnetic Shielding of a Laboratory Hall Thruster. II. Experiments", *Journal of Applied Physics*, Vol. 115, No. 4, Jan 24, 2014, pp. 043304.
https://doi.org/10.1063/1.4862314

[6] Mikellides, I. G., Hofer, R. R., Katz, I., and Goebel, D. M., "Magnetic Shielding of Hall Thrusters at High Discharge Voltages", *Journal of Applied Physics*, Vol. 116, No. 5, Aug 6, 2014, pp. 053302.
https://doi.org/10.1063/1.4892160

[7] Mazouffre, S., Tsikata, S., and Vaudolon, J., "Development and Experimental Characterization of a Wall-Less Hall Thruster", *Journal of Applied Physics*, Vol. 116, No. 24, Dec 23, 2014, pp. 243302.
https://doi.org/10.1063/1.4904965

[8] Vaudolon, J., Mazouffre, S., Hénaux, C., Harribey, D., and Rossi, A., "Optimization of a Wall-Less Hall Thruster", *Applied Physics Letters*, Vol. 107, No. 17, Oct 27, 2015, pp. 174103.
https://doi.org/10.1063/1.4932196

[9] Mazouffre, S., "Electric Propulsion for Satellites and Spacecraft: Established Technologies and Novel Approaches", *Plasma Sources Science and Technology*, Vol. 25, No. 3, Apr 6, 2016, pp. 033002.
https://doi.org/10.1088/0963-0252/25/3/033002

[10] Grimaud, L. and Mazouffre, S., "Conducting Wall Hall Thrusters in Magnetic Shielding and Standard Configurations", *Journal of Applied Physics*, Vol. 122, No. 3, Jul 21, 2017, pp. 033305.
https://doi.org/10.1063/1.4995285

[11] Garrigues, L., Santhosh, S., Grimaud, L., and Mazouffre, S., "Operation of a Low-Power Hall Thruster: Comparison between Magnetically Unshielded and Shielded Configuration", *Plasma Sources Science and Technology*, Vol. 28, No. 3, Mar 25, 2019, pp. 034003.
https://doi.org/10.1088/1361-6595/ab080d

[12] Conversano, R. W., Lobbia, R. B., Kerber, T. V., Tilley, K. C., Goebel, D. M., and Reilly, S. W., "Performance Characterization of a Low-Power Magnetically Shielded Hall Thruster with an Internally-Mounted Hollow Cathode", *Plasma Sources Science and Technology*, Vol. 28, No. 10, Oct 21, 2019, pp. 105011.
https://doi.org/10.1088/1361-6595/ab47de

[13] Duan, X., Cheng, M., Yang, X., Guo, N., Li, X., Wang, M., and Guo, D., "Investigation on Ion Behavior in Magnetically Shielded and Unshielded Hall Thrusters by Laser-Induced Fluorescence", *Journal of Applied Physics*, Vol. 127, Mar 5, 2020, pp. 093301.
https://doi.org/10.1063/1.5140514

[14] Lopez Ortega, A. and Mikellides, I. G., "The Importance of the Cathode Plume and Its Interactions with the Ion Beam in Numerical Simulations of Hall Thrusters", *Physics of Plasmas*, Vol. 23, No. 4, Apr 28, 2016, pp. 043515.
https://doi.org/10.1063/1.4947554

[15] Grimaud, L. and Mazouffre, S., "Ion Behavior in Low-Power Magnetically Shielded and Unshielded Hall Thrusters", *Plasma Sources Science and Technology*, Vol. 26, No. 5, Apr 7, 2017, pp. 055020.
https://doi.org/10.1088/1361-6595/aa660d

[16] Lopez Ortega, A., Mikellides, I. G., Sekerak, M. J., and Jorns, B. A., "Plasma Simulations in 2-D (R-Z) Geometry for the Assessment of Pole Erosion in a Magnetically Shielded Hall Thruster", *Journal of Applied Physics*, Vol. 125, No. 3, Jan 15, 2019, pp. 033302.
https://doi.org/10.1063/1.5077097

[17] Mikellides, I. G. and Lopez Ortega, A., "Growth of the Modified Two-Stream Instability in the Plume of a Magnetically Shielded Hall Thruster", *Physics of Plasmas*, Vol. 27, No. 10, Oct 5, 2020, pp. 100701.
https://doi.org/10.1063/5.0020075

[18] Huang, W. and Kamhawi, H., "Counterstreaming Ions at the Inner Pole of a Magnetically Shielded Hall Thruster", *Journal of Applied Physics*, Vol. 129, Jan 27, 2021, pp. 043305.
https://doi.org/10.1063/5.0029428

[19] Mikellides, I. G. and Lopez Ortega, A., "Growth of the Lower Hybrid Drift Instability in the Plume of a Magnetically Shielded Hall Thruster", *Journal of Applied Physics*, Vol. 129, No. 19, May 17, 2021, pp. 193301.
https://doi.org/10.1063/5.0048706

[20] Huang, W., Frieman, J. D., Kamhawi, H., Peterson, P. Y., and Hofer, R. R., "Ion Velocity Characterization of the 12.5-kW Advanced Electric Propulsion System Engineering Hall Thruster", *2021 AIAA Propulsion and Energy Forum*, AIAA-2021-3432, Virtual, Aug 9-11, 2021.
https://doi.org/10.2514/6.2021-3432

[21] Hall, S. J., Gray, T. G., Yim, J. T., Choi, M., Sarver-Verhey, T. R., and Kamhawi, H., "The Effect of Facility Background Pressure on Hollow Cathode Operation", *Journal of Applied Physics*, Vol. 130, No. 11, Sep 17, 2021, pp. 113302.
https://doi.org/10.1063/5.0061045

[22] Frieman, J. D., Gilland, J. H., Kamhawi, H., Mackey, J. A., Williams, G. J., Hofer, R. R., and Peterson, P. Y., "Wear Trends of the 12.5kW HERMeS Hall Thruster", *Journal of Applied Physics*, Vol. 130, No. 14, Oct 12, 2021, pp. 143303.
https://doi.org/10.1063/5.0062579

[23] Polk, J. E., Lobbia, R. B., Barriault, A., and Vela, P. P. G., "Use of an Accelerated Testing Method to Characterize Inner Front Pole Cover Erosion in a High Power Hall Thruster", *Journal of Applied Physics*, Vol. 130, No. 18, Nov 9, 2021, pp. 183302.
https://doi.org/10.1063/5.0067452

[24] Byers, D. and Dankanich, J. W., "A Review of Facility Effects on Hall Effect Thrusters", *31st International Electric Propulsion Conference*, 2009-076, Ann Arbor, MI, Sep 20-24, 2009.

[25] Sankovic, J. M., Hamley, J. A., and Haag, T. W., "Performance Evaluation of the Russian SPT-100 Thruster at NASA LeRC", *23rd International Electric Propulsion Conference*, 1993-094, Seattle, WA, Sep, 1993.

[26] Walker, M. L. and Gallimore, A. D., "Performance Characteristics of a Cluster of 5-kW Laboratory Hall Thrusters", *Journal of Propulsion and Power*, Vol. 23, No. 1, Jan-Feb, 2007, pp. 35-43.
https://doi.org/10.2514/1.19752

[27] Huang, W., Kamhawi, H., and Haag, T. W., "Effect of Background Pressure on the Performance and Plume of the Hivhac Hall Thruster", *33rd International Electric Propulsion Conference*, 2013-058, Washington, DC, Oct 6-10, 2013.

[28] Huang, W., Kamhawi, H., Lobbia, R. B., and Brown, D. L., "Effect of Background Pressure on the Plasma Oscillation Characteristics of the Hivhac Hall Thruster", *50th AIAA/ASME/SAE/ASEE Joint Propulsion Conference*, AIAA-2014-3708, Cleveland, OH, Jul 28-30, 2014.
https://doi.org/10.2514/6.2014-3708

[29] Diamant, K. D., Liang, R., and Corey, R. L., "The Effect of Background Pressure on SPT-100 Hall Thruster Performance", *50th AIAA/ASME/SAE/ASEE Joint Propulsion Conference*, AIAA-2014-3710, Cleveland, OH, Jul 28-30, 2014.
https://doi.org/10.2514/6.2014-3710

[30] Hofer, R. R. and Anderson, J. R., "Finite Pressure Effects in Magnetically Shielded Hall Thrusters", *50th AIAA/ASME/SAE/ASEE Joint Propulsion Conference*, AIAA-2014-3709, Cleveland, OH, Jul 28-30, 2014.
https://doi.org/10.2514/6.2014-3709

[31] Tighe, W. G., Spektor, R., and Diamant, K. D., "Effects of Background Pressure on the NASA 173M Hall Current Thruster Performance", *34th International Electric Propulsion Conference*, 2015-152, Kobe, Japan, Jul 4-10, 2015.

[32] Diamant, K. D., Curtiss, T. J., Spektor, R., Beiting, E. J., Hruby, V., Pote, B., Kolencik, J., and Paintal, S., "Performance and Plume Characterization of the BHT-1500 Hall Thruster", *34th International Electric Propulsion Conference*, 2015-069, Kobe, Japan, Jul 4-10, 2015.

[33] Frieman, J. D., "Characterization of Background Neutral Flows in Vacuum Test Facilities and Impacts on Hall Effect Thruster Operation", Ph.D. Dissertation, Aerospace Engineering, Georgia Institutde of Technology, Atlanta, GA, 2017.

[34] Snyder, J. S., Lenguito, G., Frieman, J. D., Haag, T. W., and Mackey, J. A., "Effects of Background Pressure on SPT-140 Hall Thruster Performance", *Journal of Propulsion and Power*, Vol. 36, No. 5, Sep, 2020, pp. 668-676.
https://doi.org/10.2514/1.B37702

[35] Piragino, A., Faraji, F., Reza, M., Ferrato, E., Piraino, A., and Andreussi, T., "Background Pressure Effects on the Performance of a 20 kW Magnetically Shielded Hall Thruster Operating in Various Configurations", *Aerospace*, Vol. 8, No. 69, Mar 9, 2021, pp. 1.
https://doi.org/10.3390/aerospace8030069

[36] Piragino, A., Saravia, M. M., Giannetti, V., Leporini, L., Camarri, S., Califano, F., and Andreussi, T., "The Effect of Background Neutrals and Vacuum Chamber on Performance and Plasma Characteristics on Hall Thrusters", *International Electric Propulsion Conference 2022*, 2022-320, Boston, MA, Jun 19-23, 2022.

[37] Diamant, K. D., Spektor, R., Beiting, E. J., Young, J. A., and Curtiss, T. J., "The Effects of Background Pressure on Hall Thruster Operation", *48th AIAA/ASME/SAE/ASEE Joint Propulsion Conference & Exhibit*, AIAA-2012-3735, Atlanta, GA, Jul 29-Aug 1, 2012.
https://doi.org/10.2514/6.2012-3735

[38] Huang, W., Kamhawi, H., Haag, T. W., Lopez Ortega, A., and Mikellides, I. G., "Facility Effect Characterization Test of NASA's HERMeS Hall Thruster", *52nd AIAA/SAE/ASEE Joint Propulsion Conference*, AIAA-2016-4828, Salt Lake City, UT, Jul 25-27, 2016.
https://doi.org/10.2514/6.2016-4828

[39] Yim, J. T. and Burt, J. M., "Characterization of Vacuum Facility Background Gas through Simulation and Considerations for Electric Propulsion Ground Testing", *51st AIAA/SAE/ASEE Joint Propulsion Conference*, AIAA-2015-3825, Orlando, FL, Jul 27-29, 2015.
https://doi.org/10.2514/6.2015-3825

[40] Spektor, R., Tighe, W. G., Stoltz, P. H., and Beckwith, K. R. C., "Facility Effects on Hall Thruster Performance through Cathode Coupling", *34th International Electric Propulsion Conference*, 2015-309, Kobe, Japan, Jul 4-10, 2015.

[41] Jorns, B. A. and Byrne, M. P., "Model for the Dependence of Cathode Voltage in a Hall Thruster on Facility Pressure", *Plasma Sources Science and Technology*, Vol. 30, No. 1, Jan 12, 2021, pp. 015012.

https://doi.org/10.1088/1361-6595/abd3b6

[42] Sommerville, J. D. and King, L. B., "Hall-Effect Thruster–Cathode Coupling, Part I: Efficiency Improvements from an Extended Outer Pole", *Journal of Propulsion and Power*, Vol. 27, No. 4, Jul-Aug, 2011, pp. 744-753.

https://doi.org/10.2514/1.50123

[43] Sommerville, J. D., "Hall-Effect Thruster-Cathode Coupling: The Effect of Cathode Position and Magnetic Field Topology", Ph.D. Dissertation, Mechanical Engineering, Michigan Technological University, Houghton, MI, 2009.

[44] Frieman, J. D., King, S. T., Walker, M. L., Khayms, V., and King, D. Q., "Electrical Facility Effects on Hall Thruster Cathode Coupling: Performance and Plume Properties", *Journal of Propulsion and Power*, Vol. 30, No. 6, Nov-Dec, 2014, pp. 1471-1479.

https://doi.org/10.2514/1.B35308

[45] Frieman, J. D., Walker, J. A., Walker, M. L., Khayms, V., and King, D. Q., "Electrical Facility Effects on Hall Thruster Cathode Coupling: Performance and Plume Properties", *Journal of Propulsion and Power*, Vol. 32, No. 1, Jan-Feb, 2016, pp. 251-264.

https://doi.org/10.2514/1.B35683

[46] Walker, J. A., Frieman, J. D., Walker, M. L., Khayms, V., King, D. Q., and Peterson, P. Y., "Electrical Facility Effects on Hall-Effect-Thruster Cathode Coupling: Discharge Oscillations and Facility Coupling", *Journal of Propulsion and Power*, Vol. 32, No. 4, Jul-Aug, 2017, pp. 844-855.

https://doi.org/10.2514/1.B35835

[47] Nakles, M. R. and Hargus, W. A., Jr., "Background Pressure Effects on Ion Velocity Distribution within a Medium-Power Hall Thruster", *Journal of Propulsion and Power*, Vol. 27, No. 4, Jul-Aug, 2011, pp. 737-743.

https://doi.org/10.2514/1.48027

[48] Mazouffre, S., "Laser-Induced Fluorescence Diagnostics of the Cross-Field Discharge of Hall Thrusters", *Plasma Sources Science and Technology*, Vol. 22, No. 1, Nov 29, 2013, pp. 013001.

https://doi.org/10.1088/0963-0252/22/1/013001

[49] Spektor, R., Tighe, W. G., and Kamhawi, H., "Laser Induced Fluorescence Measurements in a Hall Thruster Plume as a Function of Background Pressure", *52nd AIAA/SAE/ASEE Joint Propulsion Conference*, AIAA-2016-4624, Salt Lake City, UT, Jul 25-27, 2016.

https://doi.org/10.2514/6.2016-4624

[50] Cusson, S. E., Dale, E. T., Jorns, B. A., and Gallimore, A. D., "Acceleration Region Dynamics in a Magnetically Shielded Hall Thruster", *Physics of Plasmas*, Vol. 26, No. 2, Feb 5, 2019, pp. 023506.

https://doi.org/10.1063/1.5079414

[51] MacDonald-Tenenbaum, N., Pratt, Q., Nakles, M. R., Pilgram, N., Holmes, M., and Hargus, W. A., Jr., "Background Pressure Effects on Ion Velocity Distributions in an SPT-100 Hall Thruster", *Journal of Propulsion and Power*, Vol. 35, No. 2, Mar-Apr, 2019, pp. 403-412.
https://doi.org/10.2514/1.B37133

[52] Hargus, W. A., Jr., Tango, L. J., and Nakles, M. R., "Background Pressure Effects on Krypton Hall Effect Thruster Internal Acceleration", *33rd International Electric Propulsion Conference*, 2013-340, Washington, DC, Oct 6-10, 2013.

[53] Peterson, P. Y., Kamhawi, H., Huang, W., Yim, J. T., Herman, D. A., Williams, G. J., Gilland, J. H., and Hofer, R. R., "NASA's HERMeS Hall Thruster Electrical Configuration Characterization", *52nd AIAA/SAE/ASEE Joint Propulsion Conference*, AIAA-2016-5027, Salt Lake City, UT, Jul 25-27, 2016.
https://doi.org/10.2514/6.2016-5027

[54] Kamhawi, H., Huang, W., Haag, T. W., Yim, J. T., Herman, D. A., Peterson, P. Y., Williams, G. J., Gilland, J. H., Hofer, R. R., and Mikellides, I. G., "Performance, Facility Pressure Effects, and Stability Characterization Tests of Nasa's Hall Effect Rocket with Magnetic Shielding Thruster", *52nd AIAA/SAE/ASEE Joint Propulsion Conference*, AIAA-2016-4826, Salt Lake City, UT, Jul 25-27, 2016.
https://doi.org/10.2514/6.2016-4826

[55] Hansen, J. and Persson, W., "Revised Analysis of Singly Ionized Xenon, Xe II", *Physica Scripta*, Vol. 36, No. 4, 1987, pp. 602-643.
https://doi.org/10.1088/0031-8949/36/4/005

[56] Huang, W., "Study of Hall Thruster Discharge Channel Wall Erosion Via Optical Diagnostics", Ph.D. Dissertation, Aerospace Engineering, University of Michigan, Ann Arbor, MI, 2011.

[57] Tsikata, S., Cavalier, J., Heron, A., Honore, C., Lemoine, N., Gresillon, D., and Coulette, D., "An Axially Propagating Two-Stream Instability in the Hall Thruster Plasma", *Physics of Plasmas*, Vol. 21, No. 7, Jul 17, 2014, pp. 072116.
https://doi.org/10.1063/1.4890025

[58] Hara, K. and Treece, C., "Ion Kinetics and Nonlinear Saturation of Current-Driven Instabilities Relevant to Hollow Cathode Plasmas", *Plasma Sources Science and Technology*, Vol. 28, No. 5, May 21, 2019, pp. 055013.
https://doi.org/10.1088/1361-6595/ab18e4

[59] Hara, K. and Tsikata, S., "Cross-Field Electron Diffusion Due to the Coupling of Drift-Driven Microinstabilities", *Physical Review E*, Vol. 102, No. 2, Aug 3, 2020, pp. 023202.

https://doi.org/10.1103/PhysRevE.102.023202

[60] Frieman, J. D., Kamhawi, H., Huang, W., Mackey, J. A., Ahern, D. M., Peterson, P. Y., Gilland, J. H., Hall, S. J., Hofer, R. R., Inaba, D., Dao, H., Zubair, J., Neuhoff, J., and Branch, N. A., "Characterization Test of the 12.5-kW Advanced Electric Propulsion System Engineering Test Unit Hall Thruster", *2020 AIAA Propulsion and Energy Forum*, AIAA-2020-3626, Virtual, Aug 24-28, 2020.

https://doi.org/10.2514/6.2020-3626